Bond–slip models for FRP sheets/plates bonded to concrete

4 **AUTHORS**, INCLUDING:

Xinzheng Lu
Tsinghua University
76 PUBLICATIONS **716** CITATIONS

Bond–slip models for FRP sheets/plates bonded to concrete

X.Z. Lu[a,b], J.G. Teng[b,*], L.P. Ye[a], J.J. Jiang[a]

[a]*Department of Civil Engineering, Tsinghua University, Beijing, PR China*
[b]*Department of Civil and Structural Engineering, The Hong Kong Polytechnic University, Hong Kong, China*

Abstract

An accurate local bond–slip model is of fundamental importance in the modelling of FRP-strengthened RC structures. In this paper, a review of existing bond strength models and bond–slip models is first presented. These models are then assessed using the results of 253 pull tests on simple FRP-to-concrete bonded joints, leading to the conclusion that a more accurate model is required. In the second half of the paper, a set of three new bond–slip models of different levels of sophistication is proposed. A unique feature of the present work is that the new bond–slip models are not based on axial strain measurements on the FRP plate; instead, they are based on the predictions of a meso-scale finite element model, with appropriate adjustment to match their predictions with the experimental results for a few key parameters. Through comparisons with the large test database, all three bond–slip models are shown to provide accurate predictions of both the bond strength (i.e. ultimate load) and the strain distribution in the FRP plate.
© 2005 Elsevier Ltd. All rights reserved.

Keywords: FRP; Concrete; Bond; Bond–slip models; Bond strength; Pull tests; Finite element simulation; Composites

1. Introduction

Over the past decade, external bonding of fibre reinforced polymer (FRP) plates or sheets (referred to as plates only hereafter for brevity) has emerged as a popular method for the strengthening of reinforced concrete (RC) structures [1]. An important issue in the strengthening of concrete structures using FRP composites is to design against various debonding failure modes, including (a) cover separation [2–4]; (b) plate end interfacial debonding [2,3]; (c) intermediate (flexural or flexural-shear) crack (IC) induced interfacial debonding [5]; and (d) critical diagonal crack (CDC) induced interfacial debonding [6]. The behaviour of the interface between the FRP and the concrete is the key factor controlling debonding failures in FRP-strengthened RC structures. Therefore, for the safe and economic design of externally bonded FRP systems, a sound understanding of the behaviour of FRP-to-concrete interfaces needs to be developed. In particular,

a reliable local bond–slip model for the interface is of fundamental importance to the accurate modelling and hence understanding of debonding failures in FRP-strengthened RC structures. It should be noted that throughout this paper, the term "interface" is used to refer to the interfacial part of the FRP-to-concrete bonded joint, including the adhesive and a thin layer of the adjacent concrete, responsible for the relative slip between the FRP plate and the concrete prism, instead of any physical interface in the joint.

In various debonding failure modes, the stress state of the interface is similar to that in a pull test specimen in which a plate is bonded to a concrete prism and is subject to tension (Fig. 1). Such pull tests can be realized in laboratories in a number of ways with some variations [7], but the results obtained are not strongly dependent on the set-up as long as the basic mechanics as illustrated in Fig. 1 is closely represented [8].

The pull test not only delivers the ultimate load (referred to as the bond strength hereafter in this paper) of the FRP-to-concrete interface, but also has been used to determine the local bond–slip behaviour of the interface [9–16]. Local bond–slip curves from pull tests are commonly determined

---

* Corresponding author. Tel.: +852 2766 6012; fax: +852 2334 6389.
 E-mail address: cejgteng@polyu.edu.hk (J.G. Teng).

Notation

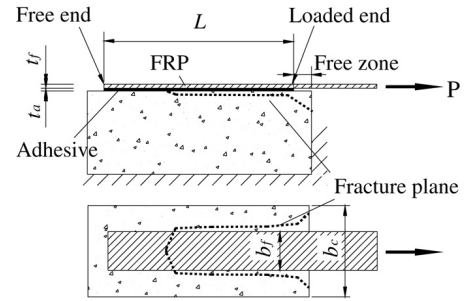|	
A, B	parameters in the proposed precise model;
b_c	width of concrete prism;
b_f	width of FRP plate;
E_a	elastic modulus of adhesive;
E_f	elastic modulus of FRP;
f'_c	concrete cylinder compressive strength;
f_t	concrete tensile strength;
G_a	shear modulus of adhesive;
G_c	elastic shear modulus of concrete;
G_f	interfacial fracture energy;
G_f^a	interfacial fracture energy for the ascending branch;
K_a	G_a/t_a, shear stiffness of adhesive layer;
K_c	G_c/t_c, shear stiffness of concrete;
L	bond length;
L_e	effective bond length;
P_u	ultimate load or bond strength;
s	local slip;
s_e	elastic component of local slip;
s_f	local slip when bond stress τ reduces to zero;
s_0	local slip at $\tau_{\max}$;
t_a	thickness of adhesive layer;
t_c	effective thickness of concrete contributing to shear deformation;
t_f	thickness of FRP plate;
$\alpha_1, \alpha_2, \alpha_3$	coefficients in proposed bond–slip models;
β_l	bond length factor;
β_w	width ratio factor;
τ	local bond stress;
$\tau_{\max}$	maximal local bond stress;
τ_u	average bond stress.

Fig. 1. Schematic of pull test.

method and has its own problem: the local bond–slip curve is determined indirectly from the load–slip curve, but it is easy to show that rather different local bond–slip curves may lead to similar load–displacement curves.

This paper has two principal objectives: (a) to provide a critical review and assessment of existing bond–slip models, and (b) to present a set of three new bond–slip models. The former part aims to clarify the differences between existing bond–slip models and between these models and test results, a task that does not appear to have been properly undertaken so far. The former part also sets the stage for the latter part in which three new bond–slip models of different levels of sophistication are presented. A unique feature of the present work is that the new bond–slip models are not based on axial strain measurements on the FRP plate, but instead they are based on the predictions of a meso-scale finite element model, with appropriate adjustment to match the experimental results of a few key parameters. As these key parameters such as the bond strength are much more reliable than local strain measurements on the FRP plate, the present approach does not suffer from the random variations associated with strain measurements nor the indirectness of the load–slip curve approach.
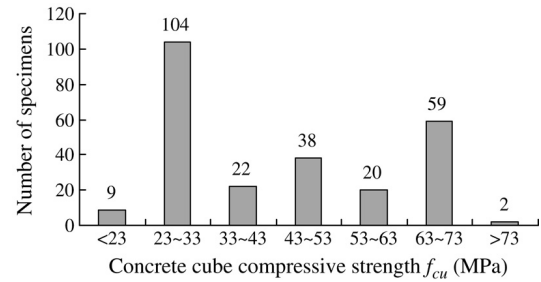
2. FRP-to-concrete bond behaviour

Before presenting a review of the existing test data and bond–slip models, some fundamental aspects of the behaviour of FRP-to-concrete interfaces should be summarized to place the present work in its proper context. Existing pull tests have shown conclusively that in the vast majority of cases and except when a very weak adhesive or a high strength concrete is used, the failure of an FRP-to-concrete bonded joint is by cracking in the concrete layer adjacent to the adhesive layer. In Fig. 1, the dotted lines identify a typical fracture plane in the process of debonding failure, and this plane is generally slightly wider than the width of the FRP plate (Fig. 1), if the plate is narrower than the concrete prism. The fracture plane propagates from the loaded end to the free end of the FRP plate as loading/deformation increases. In Fig. 1, the FRP plate is shown unbonded near the loaded end (the free zone), which has been adopted in some tests (e.g. [17]), but in some other tests, such a free zone was not included (e.g. [8,12]). If this

in two ways: (a) from axial strains of the FRP plate measured with closely spaced strain gauges (e.g. Nakaba et al. [12]); (b) from load–displacement (slip at the loaded end) curves (e.g. Ueda et al. [15]). In the first method, the shear stress of a particular location along the FRP-to-concrete interface can be found using a difference formula, while the corresponding slip can be found by a numerical integration of the measured axial strains of the plate. This method appears to be simple, but in reality cannot produce accurate local bond–slip curves. This is because the axial strains measured on the thin FRP plate generally show violent variations as a result of the discrete nature of concrete cracks, the heterogeneity of concrete and the roughness of the underside of the debonded FRP plate. For example, a strain gauge located above a crack will have a much greater strain than one that sits above a large aggregate particle. The shear stress deduced from such axial strains is thus not reliable although the slip is less sensitive to such variations. Consequently, bond–slip curves found from different tests may differ substantially. The second method is an indirect

free zone does not exist or is small, a lump of concrete near the loaded end will generally be pulled off the concrete prism, but this variation in detail does not have a significant effect on the local bond–slip behaviour elsewhere nor the general behaviour as long as the bond length is not very short. From existing theoretical and experimental studies (e.g. [7,15,16]), the following six parameters are known to govern the local bond–slip behaviour as well as the bond strength of FRP-to-concrete bonded joints in pull tests: (a) the concrete strength, (b) the bond length L (Fig. 1), (c) the FRP plate axial stiffness, (d) the FRP-to-concrete width ratio, (e) the adhesive stiffness, and (f) the adhesive strength. A very important aspect of the behaviour of these bonded joints is that there exists an effective bond length L_e beyond which an extension of the bond length L cannot increase the ultimate load. This is a fundamental difference between an externally bonded plate and an internal reinforcing bar for which a sufficiently long anchorage length can always be found so that the full tensile strength of the reinforcement can be achieved.
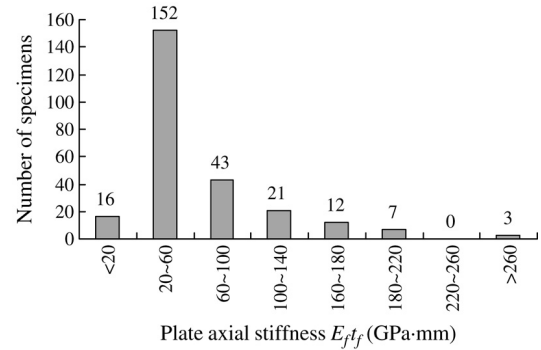
3. Existing pull tests

In this study, a database containing the results of 253 pull tests on FRP-to-concrete bonded joints was built. The database includes tests reported by Chajes et al. [18], Taljsten [19], Takeo et al. [20], Zhao et al. [21], Ueda et al. [22], Nakaba et al. [12], Wu et al. [13], Tan [17], Ren [23] and Yao et al. [8]. Both single shear tests (e.g. Yao et al. [8]) and double shear tests (e.g. Tan [17]) are included in the database. Details of these tests, except those already included in the easily accessible databases assembled by Chen and Teng [7], Nakaba et al. [12] and those from the recent study of Yao et al. [8], are given in Table A.1 of Appendix A, where b_f, t_f, E_f and f_f are the width, thickness, elastic modulus and tensile strength of the FRP plate respectively, b_c is the width of the concrete prism, f_{cu} is the cube compressive strength of concrete (converted from cylinder compressive strength by a factor of 0.78 where applicable), f_t is the tensile strength of concrete ($f_t = 0.395 f_{cu}^{0.55}$ according to the Chinese code for the design of concrete structures [24] if not available from the original source), L is the total bond length, and P_u is the bond strength. For some of these specimens, strains measured on the FRP plate are also available.
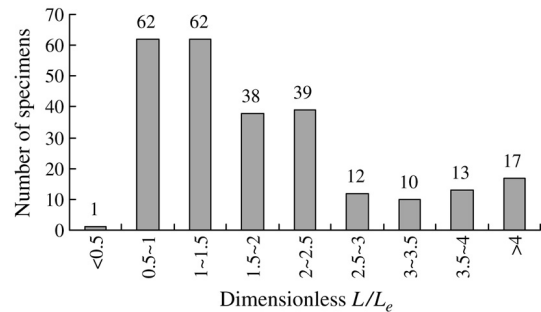
The distributions of the test data in terms of the following four key parameters are shown in Fig. 2: (a) the concrete cube compressive strength (Fig. 2(a)); (b) the axial stiffness of the plate per unit width (Fig. 2(b)); (c) the bond length normalized by the effective bond length predicted by Chen and Teng's model [7]; (d) the FRP plate-to-concrete prism width ratio. It is clear that the test data cover a wide range of each parameter and can be expected to provide a reliable benchmark for theoretical models. It is desirable for future tests to be conducted in regions where current data are scarce.

(a) Range of concrete strength.

(b) Range of plate stiffness.

(c) Range of bond length.

(d) Range of FRP-to-concrete width ratio.

Fig. 2. Distributions of test data in terms of key parameters.

Dai and Ueda [14] and Ueda et al. [15] recently reported that the bond strength of FRP-to-concrete interfaces can be enhanced through the use of a very soft adhesive layer with a shear stiffness K_a ($=G_a/t_a$) being between 0.14 and 1.0 GPa/mm, where t_a is the adhesive layer thickness and G_a is the elastic shear modulus of the adhesive. It is clear that a small shear stiffness of the adhesive layer can be achieved by the use of a soft adhesive or a thick adhesive layer. While the properties of the adhesives used in

the specimens of the present test database were not always reported, none of the relevant studies was focussed on the issue of very soft adhesive layers. At least outside Japan, the application of adhesives commonly available in the market in a procedure complying with the recommendations of the manufacturers is unlikely to lead to an adhesive layer which can be classified as being very soft (i.e. with a shear stiffness in the range studied by Dai and Ueda [14] and Ueda et al. [15]). Furthermore, relatively soft adhesives are normally used only in wet lay-up applications where the definition of the thickness of the adhesive layer is problematic but affects the value of the shear stiffness of the adhesive layer significantly. Indeed, since the same resin is commonly used to saturate the fibre sheet to form the FRP plate as well as to bond the FRP plate to the concrete which is often already covered with a thin layer of primer, the thickness of the adhesive layer which deforms primarily in shear cannot be easily defined and is believed to be very small by the present authors in debonding failures unless debonding occurs in the adhesive layer. Finally, in practice, the thickness of the adhesive layer cannot be precisely controlled and measured as reported in the studies of Dai and Ueda [14] and Ueda et al. [15]. Therefore, it is reasonable to assume that the bonded joints of the present database have K_a values much greater than those studied by Dai and Ueda [14] and Ueda et al. [15] and are referred to as normal-adhesive joints hereafter. A separate study by the authors to be reported in a future paper has shown that for values of K_a ranging from 2.5 to 10 GPa/mm the bond–slip curve is little dependent on the shear stiffness of the adhesive layer. A shear stiffness of 5 GPa/mm for the shear-deformed adhesive layer is used in this study to represent a normal-adhesive bonded joint when it is needed. As the bond–slip models of Dai and Ueda [14] and Ueda et al. [15] are for very soft adhesive layers and consider the adhesive layer shear stiffness as a significant parameter, they are not included in the comparisons and discussions in this paper. The test data from their studies are also not included in the present database. The scope of the present study is therefore limited to FRP-to-concrete bonded joints whose shear-deformed adhesive layer has a shear stiffness of no less than 2.5 GPa/mm. The present work nevertheless is believed to cover at least all commercially available FRP systems for external bonding applications outside Japan.

4. Existing theoretical models for bond behaviour

4.1. Bond strength models

Many theoretical models have been developed from 1996 onwards to predict the bond strengths of FRP-to-concrete bonded joints, generally on the basis of pull test results. These are commonly referred to as bond strength models. Altogether 12 bond strength models have been found in the existing literature, and eight of them have been examined in detail by Chen and Teng [7]. These eight

models have been developed by Tanaka [25], Hiroyuki and Wu [26], van Gemert [27,28], Maeda et al. [9], Neubauer and Rostasy [29], Khalifa et al. [30], Chaallal et al. [31] and Chen and Teng [7]. The four models not covered by Chen and Teng [7] include three models (Izumo, Sato, and Iso) developed in Japan and described in a recent JCI report [32] and one developed by Yang et al. [33]. These four models are detailed in Appendix B. Table 1 provides a summary of the key parameters considered by these 12 models, while an assessment of their accuracy is given later in the paper.

4.2. Bond–slip models

Despite the difficulty in obtaining local bond–slip curves from pull tests directly, local bond–slip models for FRP-to-concrete interfaces have been developed, based on strain measurements or load–slip curves. Six local bond–slip models available in the existing literature are summarized in Table 2, where τ (MPa) is the local bond (shear) stress, s (mm) is the local slip, τ_{max} (MPa) is the local bond strength (i.e. the maximum bond/shear stress experienced by the interface), s_0 (mm) is the slip when the bond stress reaches τ_{max}, s_f (mm) is the slip when the bond stress reduces to zero, β_w is the width ratio factor, f_c' (MPa) is the cylinder compressive strength of concrete. In addition, Sato [32] proposed a model which was modified from an existing bond–slip model for rebar-concrete interfaces by replacing the yield strain of steel with the ultimate tensile strain of FRP, based on strain measurements on FRP-strengthened RC tension members. As a result, the model has included the effect of tensile cracking and is not a true local bond–slip model. This model is therefore not further discussed in this paper. Of the six models, the two models recently proposed by Dai and Ueda [14] and Ueda et al. [15] were based on test data for specimens with very soft adhesive layers and are not further discussed in this paper.

5. Accuracy of existing theoretical models

5.1. Bond strength models

The predictions of all 12 bond strength models are compared with the 253 test results of the present test database in Table 3 and Fig. 3. The average value and coefficient of variation of the predicted-to-test bond strength ratios and the correlation coefficient of each model are given in Table 3. It can be seen that the bond strength models of Maeda et al. [9], Neubauer and Rostasy [29], Khalifa et al. [30], Iso [32], Yang et al. [33] and Chen and Teng [7] are the better models, with a reasonably small coefficient of variation and a large correlation coefficient. The test results are shown against the predictions of these better-performing models in Fig. 3. Based on Tables 1 and 3 as well as Fig. 3, Chen and Teng's model is clearly the most accurate model among the 12 existing bond strength models. If Table 3 is examined together with Table 1, it can be found that the

Table 1
Factors considered by existing bond strength models

	Bond strength model	Concrete strength	FRP plate stiffness	Effective bond length	Width ratio
1	Tanaka [25]	No	No	No	No
2	Hiroyuki and Wu [26]	No	No	No	No
3	van Gemert [27]	Yes	No	No	No
4	Maeda et al. [9]	Yes	Yes	Yes	No
5	Neubauer and Rostasy [29]	Yes	Yes	Yes	Yes
6	Khalifa et al. [30]	Yes	Yes	Yes	No
7	Chaallal et al. [31]	No	Yes	No	No
8	Chen and Teng [7]	Yes	Yes	Yes	Yes
9	Izumo [32]	Yes	Yes	No	No
10	Sato [32]	Yes	Yes	Yes	No
11	Iso [32]	Yes	Yes	Yes	No
12	Yang et al. [33]	Yes	Yes	Yes	No

accuracy of a model improves as more significant parameters are considered, with the effective bond length being the most influential parameter. All the six better-performing models include a definition of the effective bond length. Of the other six models, only Sato's model [32] takes the effective bond length into consideration.

5.2. Shapes of bond–slip models

For a bond–slip model to provide accurate predictions, it needs to have an appropriate shape as well as a correct value for the interfacial fracture energy which is equal to the area under the bond–slip curve. The shape of the bond–slip model determines the predicted distribution of axial strains in the plate. The predictions of the four existing bond–slip models for normal-adhesive interfaces are shown in Fig. 4 for an FRP-to-concrete bonded joint with the following properties: $f'_c = 32$ MPa, $f_t = 3.0$ MPa, $b_f = 50$ mm, $b_c = 100$ mm, $E_f t_f = 16.2$ GPa mm. An FRP-to-concrete width ratio of 0.5 was chosen for this comparison joint as some of the bond–slip models were based on test results of joints with similar width ratios and do not account for the effect of varying this ratio. It can be seen that the shapes of the predicted bond–slip curves differ substantially (Fig. 4). In particular, the linear-brittle model of Neubauer and Rostasy [34] is very different from the other three models. The fact that the bond stress reduces to zero at the ultimate slip dictates that there exists an effective bond length beyond which an increase in the bond length will not increase the ultimate load.

Existing studies (e.g. [12,36]) have shown that the bond–slip curve should have an ascending branch and a descending branch, similar to the curve from Nakaba et al.'s model [12] or Savioa et al.'s model [36] shown in Fig. 4. The bilinear model can be used as an approximation [16], but the linear-brittle model by Neubauer and Rostasy [34] is unrealistic. Apart from the general shape, three key parameters, including the maximum bond stress, the slip at maximum stress and the ultimate slip at zero bond stress,

determine the accuracy of the model. It is interesting to note that the models by Nakaba et al. [12], Monti et al. [35] and Savioa et al. [36] are in reasonably close agreement, and the linear-brittle model of Neubauer and Rostasy [34] predicts a similar maximum bond stress. It should be noted that Savioa et al.'s model [36] was obtained by some very minor modifications of Nakaba et al.'s model (Table 2).

5.3. Interfacial fracture energy of bond–slip models

Existing research has shown that the bond strength P_u of an FRP-to-concrete bonded joint is directly proportional to the square root of the interfacial fracture energy $\sqrt{G_f}$ regardless of the shape of the bond–slip curve [16,29,37, 38], so a comparison of the bond strength is equivalent to a comparison of the interfacial fracture energy. As most bond–slip models do not provide an explicit formula for the ultimate load, the bond strengths of bond–slip models need to be obtained numerically. In the present study, they were obtained by numerical nonlinear analyses using MSC.Marc [39] with a simple model consisting of 1 mm long truss elements representing the FRP plate connected to a series of shear springs on a rigid base representing the bond–slip law of the interface. The nonlinear analyses were carried out with a tight convergence tolerance to ensure accurate predictions. The theoretical predictions of the bond strengths are compared with the 253 test results of the present test database. The average value and coefficient of variation of the predicted-to-test bond strength ratios together with the correlation coefficient for each model are given in Table 4. The correlation coefficients for all four bond–slip models are larger than 0.8, which demonstrates that the trends of the test data are reasonably well described by the bond–slip models. The coefficients of variation of these models are nevertheless still larger than that of Chen and Teng's model (Table 3). The test results are shown against the theoretical predictions in Fig. 5, where it is clearly seen that all four bond–slip models are too optimistic.

Table 2
Existing bond–slip models

Bond–slip model	Ascending branch $s \leq s_0$	Descending branch $s > s_0$	τ_{max}	s_0	s_f	β_w	Remarks
Neubauer and Rostasy [34]	$\tau_{max}\left(\frac{s}{s_0}\right)$	0	$1.8\beta_w f_t$	$\beta_w \times 0.202$		$\sqrt{1.125\frac{2-b_f/b_c}{1+b_f/400}}$	A linear ascending branch and a sudden drop
Nakaba et al. [12]	$\tau_{max}\left(\frac{s}{s_0}\right)\left[3/\left(2+\left(\frac{s}{s_0}\right)^3\right)\right]$		$3.5 f_c'^{0.19}$	0.065			A single curve
Monti et al. [35]	$\tau_{max}\frac{s}{s_0}$	$\tau_{max}\frac{s_f-s}{s_f-s_0}$	$1.8\beta_w f_t$	$2.5\tau_{max}\left(\frac{t_a}{E_a}+\frac{50}{E_c}\right)$	$0.33\beta_w$	$\sqrt{\frac{1.5(2-b_f/b_c)}{1+b_f/100}}$	
Savioa et al. [36]	$\tau_{max}\left(\frac{s}{s_0}\right)\left[2.86/\left(1.86+\left(\frac{s}{s_0}\right)^{2.86}\right)\right]$		$3.5 f_c'^{0.19}$	0.051			A single curve
Dai and Ueda [14][a]	$\tau_{max}\left(\frac{s}{s_0}\right)^{0.575}$	$\tau_{max}e^{-\beta(s-s_0)}$	$\frac{-1.575\alpha K_a+\sqrt{2.481\alpha^2 K_a^2+6.3\alpha\beta^2 K_a G_f}}{2\beta}$	$\tau_{max}/(\alpha K_a)$		$\alpha = 0.028(E_f t_f/1000)^{0.254}$, $\beta = 0.0035 K_a(E_f t_f/1000)^{0.34}$, $K_a = G_a/t_a$, $G_f = 7.554 K_a^{-0.449}(f_c')^{0.343}$	
Ueda et al. [15][a]	$2UG_f(e^{-Us}-e^{-2Us})[U = 6.846(E_f t_f/1000)^{0.108}(G_a/t_a/1000)^{0.833}, G_f = 0.446(E_f t_f/1000)^{0.023}(G_a/t_a/1000)^{-0.352} f_c'^{0.236}]$						A single curve

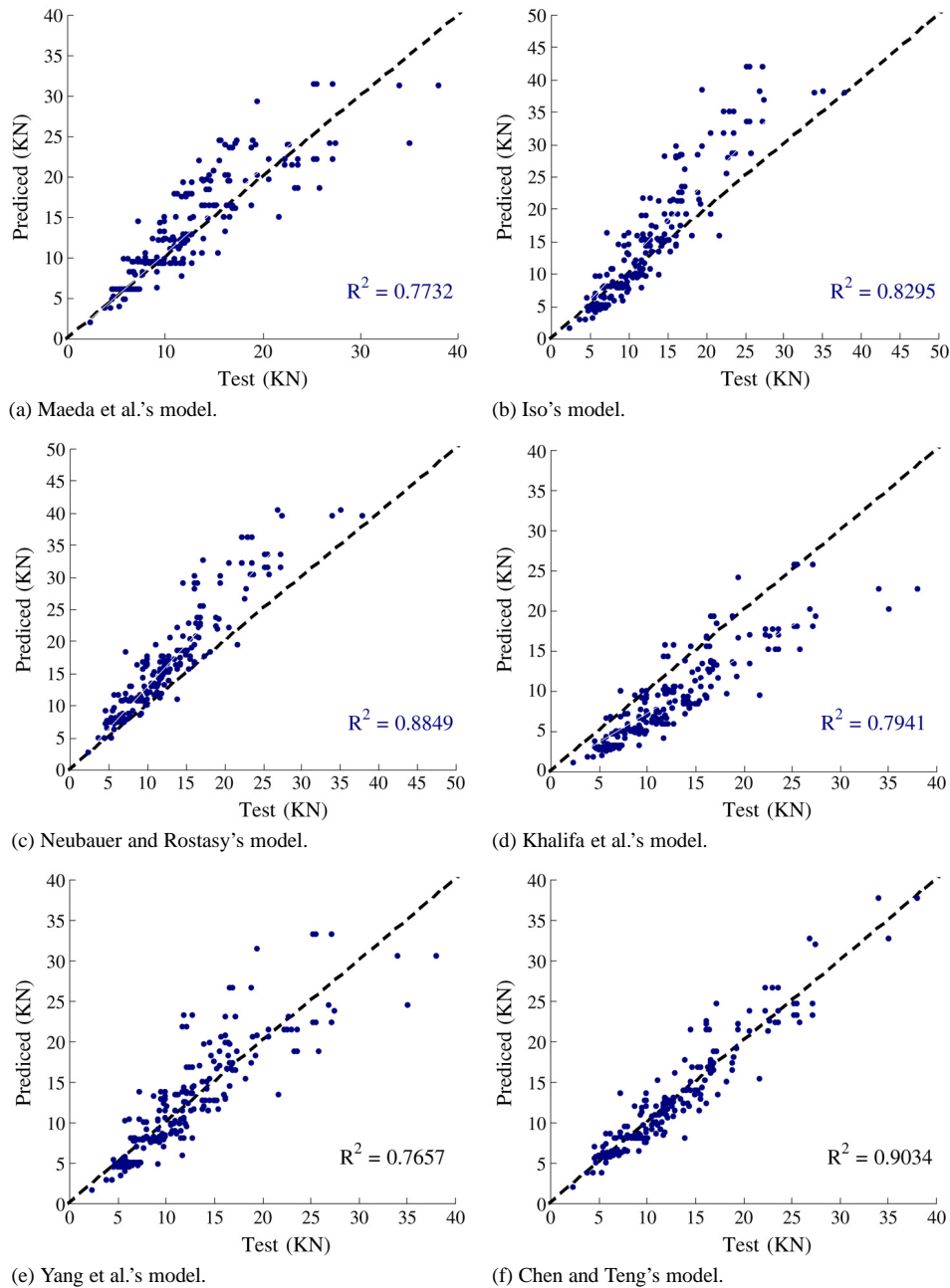[a] Regressed from specimens with very soft adhesive layers.

Fig. 3. Test bond strengths versus predictions of existing bond strength models.

6. Meso-scale finite element model

Since it is difficult to obtain accurate bond–slip curves directly from strain measurements in a pull test, Lu et al. [40] recently explored a numerical approach from which the bond–slip curve of any point along the interface can be obtained. The approach is based on the observation that debonding in a pull test occurs in the concrete, so if the failure of concrete can be accurately modelled, the interfacial shear stress and slip at a given location along the interface can be obtained from the finite element model. It should be noted that this numerical modelling approach

relies on the accurate modelling of concrete failure near the adhesive layer. Tests have shown that debonding of FRP from concrete in a pull test generally occurs within a thin layer of concrete of 2 to 5 mm thick adjacent to the adhesive layer. To simulate concrete failure within such a thin layer, with the shapes and paths of the cracks properly captured, Lu et al. [40] proposed a meso-scale finite element approach in which very small elements (with element sizes being one order smaller than the thickness of the facture zone of concrete) are used in conjunction with a fixed angle crack model (FACM) [41]. The size effect of elements is duly accounted for through fracture energy considerations. This

Table 3
Predicted-to-test bond strength ratios: bond strength models

	Bond strength model	Average Predicted-to-test bond strength ratio	Coefficient of variation	Correlation coefficient
1	Tanaka [25]	4.470	0.975	0.481
2	Hiroyuki and Wu [26]	4.290	0.611	−0.028
3	Sato [32]	1.954	0.788	0.494
4	Chaallal et al. [31]	1.683	0.749	0.240
5	Khalifa et al. [30]	0.680	0.293	0.794
6	Neubauer and Rostasy [29]	1.316	0.168	0.885
7	Izumo [32]	1.266	0.506	0.656
8	van Gemert [27]	1.224	0.863	0.328
9	Maeda et al. [9]	1.094	0.202	0.773
10	Iso [32]	1.087	0.282	0.830
11	Yang et al. [33]	0.996	0.263	0.766
12	Chen and Teng [7]	1.001	0.163	0.903
13	Proposed strength formula (Eq. (4e))	1.001	0.156	0.908

Table 4
Predicted-to-test bond strength ratios: bond–slip models

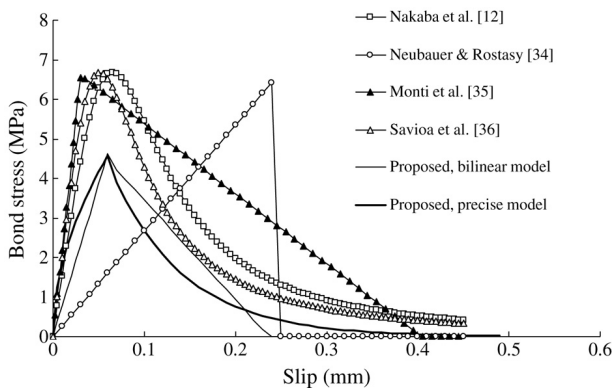|	Bond–slip model	Average predicted-to-test bond strength ratio	Coefficient of variation	Correlation coefficient
1	Neubauer and Rostasy [34]	1.330	0.209	0.887
2	Nakaba et al. [12]	1.326	0.231	0.846
3	Savioa et al. [36]	1.209	0.199	0.847
4	Monti et al. [35]	1.575	0.164	0.888
5	Proposed, precise model	1.001	0.155	0.910
6	Proposed, simplified model	1.001	0.155	0.910
7	Proposed, bilinear model	1.001	0.156	0.908

Fig. 4. Bond–slip curves from existing bond–slip models.

approach has the simplicity of the FACM for which the relevant material parameters have clear physical meanings and can be found from well established standard tests, but in the meantime retains the capability of tracing the paths of cracks as deformations increase through the use of very small elements. To reduce the computational effort, the three-dimensional FRP-to-concrete bonded joint (Fig. 1) was modelled as a plane stress problem using four-node isoparametric elements, with the effect of FRP-to-concrete width ratio being separately considered using a width ratio factor devised by Chen and Teng [7].
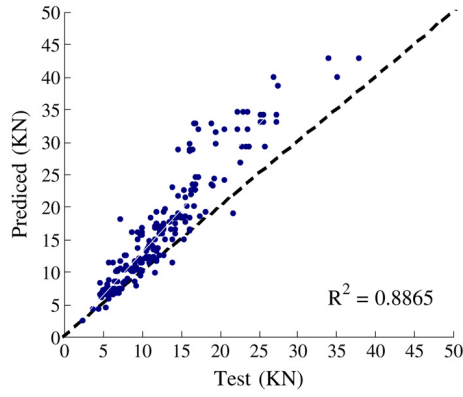
Lu et al. [40] implemented their finite element model into the general purpose finite element package MSC.Marc [39] as a user subroutine. The finite element model was verified by detailed comparisons with the results of 10 pull tests taken from studies by Wu et al. [13], Ueda et al. [22], Tan [17], and Yuan et al. [16]. A close agreement was achieved for all 10 specimens. A Fast Fourier Transform smoothing procedure was proposed in Lu et al. [40] to process the raw finite element interfacial shear stresses before the results are used to obtain local bond–slip curves. Lu et al. [40] showed that a smoothing length of 10 mm is suitable and this length was used in the present study. An unbonded zone of 25 mm was included in the finite element model in all numerical simulations of the present study. Further details of the finite element model can be found in Lu et al. [40].

7. Proposed bond–slip models

7.1. Precise model

Using the meso-scale finite element model of Lu et al. [40], a parametric study was undertaken to study the local bond–slip behaviour of the interface, considering the effects of a number of key parameters. The bonded joint modelled in this parametric study has the following properties: the axial stiffness of the FRP plate $E_f t_f$ is 26 GPa mm, which is similar to that provided by one thin layer of CFRP and is within the most popular range of FRP

(a) Neubauer and Rostasy's model.

(b) Nakaba et al.'s model.

(c) Monti et al.'s model.

(d) Savioa et al.'s model.

Fig. 5. Test bond strengths versus predictions of existing bond–slip models.
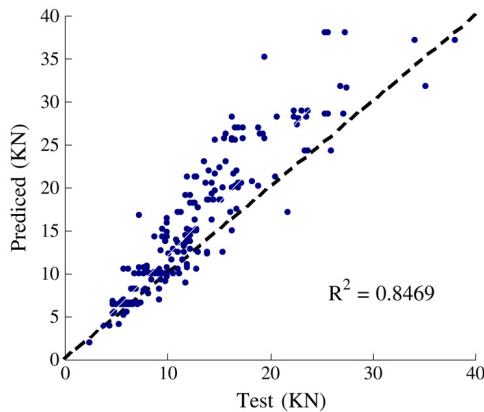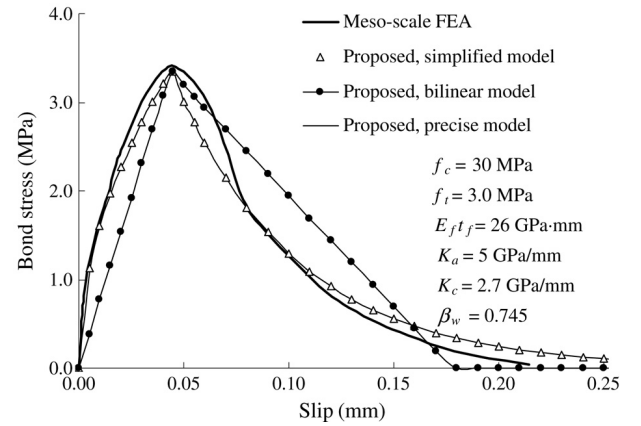

Fig. 6. Bond–slip curves from meso-scale finite element simulation and proposed bond–slip models.

plate axial stiffness in pull tests (Fig. 2(b)). In the finite element analysis, the elastic modulus E_c, tensile strength f_t and compressive strength f_c of concrete were related to the cube compressive strength of concrete according to the Chinese code for the design of concrete structures [24]: $E_c = \frac{100\,000}{2.2+34.74/f_{cu}}$, $f_t = 0.395(f_{cu})^{0.55}$ and $f_c = 0.76 f_{cu}$, all in MPa. The Poisson ratio was assumed to be 0.2. The shear stiffness of the adhesive layer is 5 GPa/mm. The bond length of the FRP plate is 200 mm, which is much longer than the effective bond length. A typical bond–slip curve obtained from the finite element model is shown in Fig. 6. From these finite element results, the following observations can be made:

(a) The bond–slip curve is made up of an ascending branch and a descending branch, with the bond stress reducing to zero when the slip is sufficiently large.

(b) The initial stiffness of the bond–slip curve is much larger than the secant stiffness at the peak stress point. This initial high stiffness, representing the stiffness of the completely linear elastic state of the interface, decreases quickly with the appearance of micro-cracking in the concrete as the bond stress increases.

(c) The maximum bond stress $\tau_{\max}$ and the corresponding slip s_0 increase almost linearly with f_t, while the interfacial fracture energy G_f increases almost linearly with $\sqrt{f_t}$, as shown in Fig. 7.

Based on the above observations, the following equations, referred to hereafter as the precise bond–slip model, are proposed to describe the local bond–slip relationship:

$$\tau = \tau_{\max}\left(\sqrt{\frac{s}{s_0 A} + B^2} - B\right) \qquad \text{if } s \le s_0 \qquad (1a)$$

$$\tau = \tau_{\max} \exp[-\alpha(s/s_0 - 1)] \qquad \text{if } s > s_0, \qquad (1b)$$

where $A = (s_0 - s_e)/s_0$, $B = s_e/[2(s_0 - s_e)]$. To closely capture the finite element bond–slip curves, a variety of equation forms were tested and Eqs. (1a) and (1b) were found to predict the finite element bond–slip curves most closely without undue complexity. The maximum bond
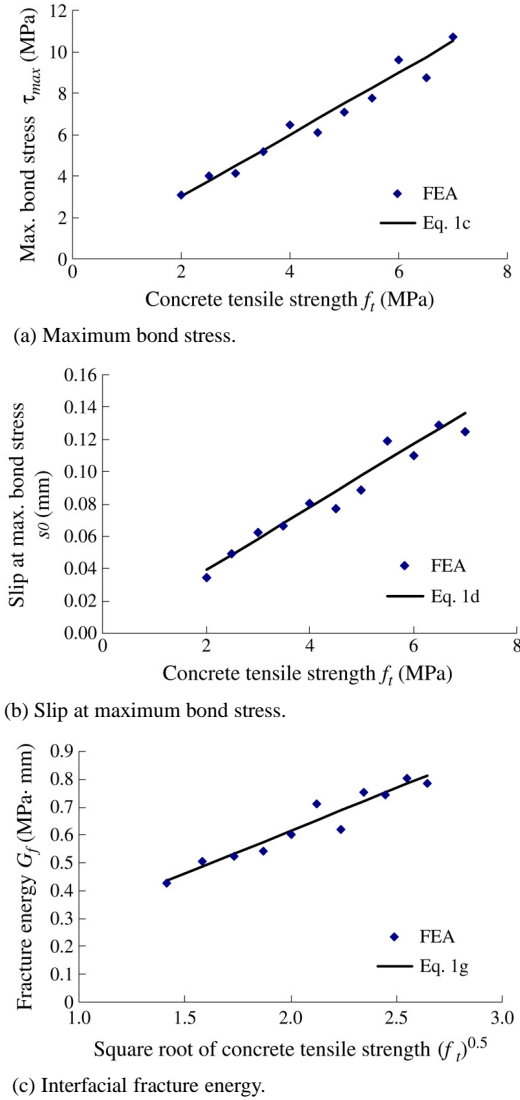
(a) Maximum bond stress.

(b) Slip at maximum bond stress.

(c) Interfacial fracture energy.

Fig. 7. Relationships between key bond–slip parameters and concrete tensile strength.

Fig. 8. Initial stiffness of bond–slip curve.

more deliberation, the overall effect of such precision on the bond–slip curve is very small and insignificant for practical purposes. Furthermore, it may be noted that the simplified model introduced below does not include t_c as a parameter but still leads to a bond–slip curve which is very closely similar to that of the precise model.

The parameter α in Eq. (1b) controls the shape of the descending branch and is given by

$$\alpha = \tau_{\max} s_0 / (G_f - G_f^a) \tag{1f}$$

where the interfacial fracture energy can be expressed as:

$$G_f = \alpha_3 \beta_w^2 \sqrt{f_t} f(K_a) \tag{1g}$$

while the fracture energy of the ascending branch G_f^a can be calculated as:

$$G_f^a = \int_0^{s_0} \tau \, ds = \tau_{\max} s_0$$
$$\times \left[\frac{2A}{3} \left(\frac{1 + B^2 A}{A} \right)^{3/2} - B - \frac{2}{3} B^3 A \right]. \tag{1h}$$

It should be noted that Eqs. (1c), (1d) and (1g) were found as linear best-fit lines to the finite element predictions, except for the introduction of the width effect ratio β_w and the elastic slip component s_e. The width effect is introduced based on existing knowledge of how it affects the three bond–slip parameters defined by Eqs. (1c), (1d) and (1g), while the elastic slip component is introduced to ensure that the slope of the bond–slip model is equal to that given by Eq. (1e). The elastic slip component is generally very small and its inclusion in Eq. (1d) has little effect on its predictions. The function $f(K_a)$ is included to cater for the future extension of the model to interfaces with very soft adhesive layers but for normal adhesive layers with $K_a \geq 2.5$ GPa/mm, $f(K_a) = 1$ as finite element results not presented here have shown that the effect of the adhesive layer stiffness on G_f is very small for such normal adhesives.

Because of some inevitable differences between the finite element predictions and the test results, the three coefficients

stress $\tau_{\max}$ and the corresponding slip s_0 are given by

$$\tau_{\max} = \alpha_1 \beta_w f_t \tag{1c}$$
$$s_0 = \alpha_2 \beta_w f_t + s_e \tag{1d}$$

where $s_e = \tau_{\max} / K_0$ is the elastic component of s_0 and β_w is the FRP-to-concrete width ratio factor. The initial stiffness of the bond–slip model is defined by

$$K_0 = K_a K_c / (K_a + K_c) \tag{1e}$$

where $K_a = G_a / t_a$ and $K_c = G_c / t_c$. G_c is the elastic shear modulus of concrete and t_c is the effective thickness of the concrete whose deformation forms part of the interfacial slip, which can be deduced from the initial stiffness of the bond–slip curve from a meso-scale FE analysis [40]. The initial part of the bond–slip curve from meso-scale FE analysis given in Fig. 6 is shown in Fig. 8. It can be seen that $t_c = 5$ mm leads to a close prediction of the bond–slip curve. While a precise definition of t_c requires
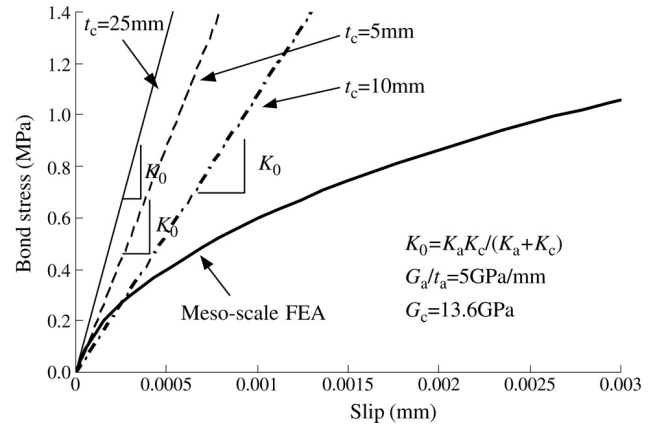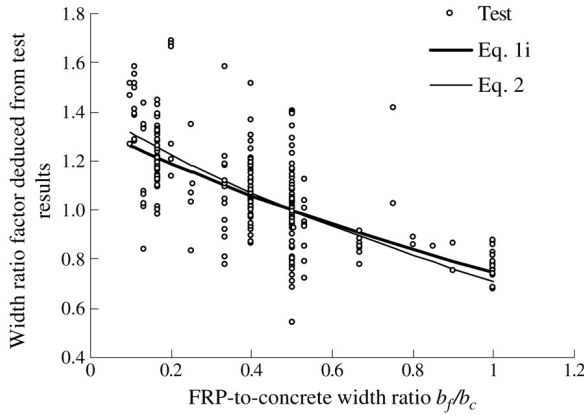
Fig. 9. Evaluation of the FRP-to-concrete width ratio effect.

in the proposed bond–slip model α_1, α_2 and α_3 were determined through an iterative procedure, making use of both the finite element and the test results. The planar nature of the finite element model also means that the effect of the FRP-to-concrete width ratio needs to be accounted for based on the test results. This iterative procedure is as follows:

(1) Take $K_a = 5$ GPa/mm for a normal adhesive layer and start the process with $\alpha_1 = 1.5$, $\alpha_2 = 0.02$ and $\alpha_3 = 0.3$, which were determined from regressions of the finite element results.
(2) Assuming that $\beta_w = 1$, use the precise bond–slip model with the coefficients from step (1) to calculate the bond strength.
(3) Compare the predicted bond strengths with the test results to evaluate the width ratio effect and to determine a best-fit expression for the width ratio factor β_w. Fig. 9 shows the deduced values of the width ratio factor at the end of the iterative process.
(4) Using the current expression for β_w, fine-tune the values for α_1, α_2 and α_3 to reach an improved agreement between the predicted and the test bond strengths.
(5) Compare the predicted bond strengths to the test results again to refine the expression for β_w.
(6) Repeat steps (4) and (5) until changes in α_1, α_2 and α_3 fall below 0.1%.

The final values obtained from this process for these three coefficients are: $\alpha_1 = 1.50$, $\alpha_2 = 0.0195$, and $\alpha_3 = 0.308$, while the width ratio factor is given by

$$\beta_w = \sqrt{\frac{2.25 - b_f/b_c}{1.25 + b_f/b_c}}. \tag{1i}$$

The bond–slip curve from the precise model for one of the bonded joints analysed by the finite element method is shown in Fig. 6. It is clear that there is a close agreement between this precise model and the finite element curve.

In terms of the present test database, Eq. (1i) represents a slight improvement to the following expression originally

proposed by Chen and Teng [7]:

$$\beta_w = \sqrt{\frac{2 - b_f/b_c}{1 + b_f/b_c}}. \tag{2}$$

The difference between the two expressions is however very small (Fig. 9) and both equations are satisfactory for practical applications.

7.2. Simplified model

The precise model is accurate but somewhat complicated. A simplified model without a significant loss of accuracy can be easily obtained by noting that the initial stiffness of the bond–slip curve is much larger than the secant stiffness at the peak point. Based on this observation, the initial stiffness can be approximated as infinity and the following simplified bond–slip model can be obtained:

$$\tau = \tau_{\max}\sqrt{\frac{s}{s_0}} \qquad \text{if } s \le s_0 \tag{3a}$$

$$\tau = \tau_{\max}e^{-\alpha\left(\frac{s}{s_0}-1\right)} \qquad \text{if } s > s_0 \tag{3b}$$

where

$$s_0 = 0.0195\beta_w f_t \tag{3c}$$

$$G_f = 0.308\beta_w^2\sqrt{f_t} \tag{3d}$$

$$\alpha = \frac{1}{\frac{G_f}{\tau_{\max}s_0} - \frac{2}{3}}. \tag{3e}$$

$\tau_{\max}$ and β_w can be calculated with Eqs. (1c) and (1i). The bond–slip curve predicted by the simplified model is also shown in Fig. 6, where it can be seen that there is little difference between this model and the precise model. For all practical purposes, the simplified model is sufficient for normal-adhesive joints with $f(K_a) = 1$ but much simpler than the precise model.

7.3. Bilinear model

Further simplification can be made to the simplified model by adopting a bilinear bond–slip curve which can be used to derive a simple explicit design equation for the bond strength. This bilinear model has the same local bond strength and total interfacial fracture energy, so the bond strength is unaffected by this simplification if the bond length is longer than the effective bond length. This bilinear model is described by the following equations:

$$\tau = \tau_{\max}\frac{s}{s_0} \qquad \text{if } s \le s_0 \tag{4a}$$

$$\tau = \tau_{\max}\frac{s_f - s}{s_f - s_0} \qquad \text{if } s_0 < s \le s_f \tag{4b}$$

$$\tau = 0 \qquad \text{if } s > s_f \tag{4c}$$
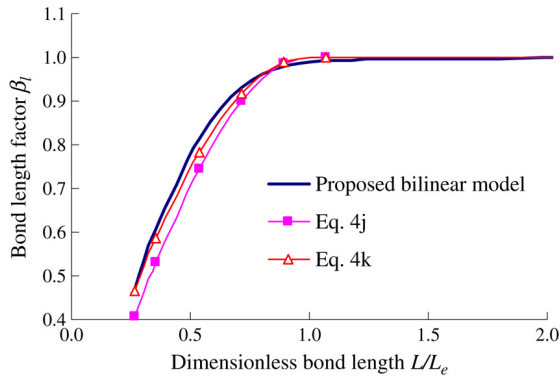
where

$$s_f = 2G_f/\tau_{\max}. \tag{4d}$$

Fig. 10. Bond length factor versus bond length.

(a) Precise model.

(b) Bilinear model.

Fig. 11. Bond strengths: test results versus predictions of proposed bond–slip models.

In the above equations, τ_{max}, s_0 and G_f can be found using Eqs. (1c), (3c) and (3d), respectively. The prediction of the bilinear model is also shown in Fig. 6.

Regardless of the bond–slip model, the bond strength of an FRP-to-concrete bonded joint in terms of the interfacial fracture energy is given by Eq. (4e) [16]

$$P_u = \beta_l b_f \sqrt{2 E_f t_f G_f} \qquad (4e)$$

where β_l is the bond length factor. When $L > L_e$, $\beta_l = 1$, but when $L < L_e$, β_l is smaller than 1. The analytical solution for L_e with a bilinear bond–slip model is given by Yuan et al. [16]:

$$L_e = a + \frac{1}{2\lambda_1} \ln \frac{\lambda_1 + \lambda_2 \tan(\lambda_2 a)}{\lambda_1 - \lambda_2 \tan(\lambda_2 a)} \qquad (4f)$$

where

$$\lambda_1 = \sqrt{\frac{\tau_{max}}{s_0 E_f t_f}} \qquad (4g)$$

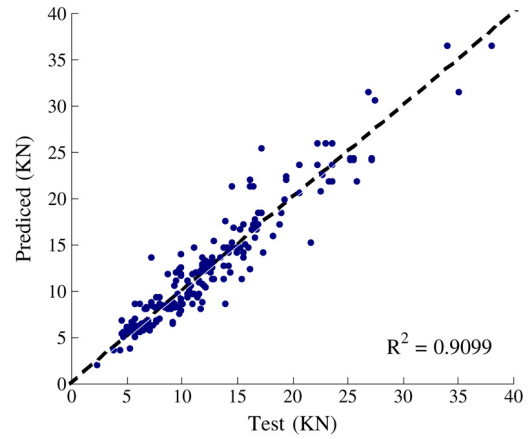$$\lambda_2 = \sqrt{\frac{\tau_{max}}{(s_f - s_0) E_f t_f}} \qquad (4h)$$

$$a = \frac{1}{\lambda_2} \arcsin\left[0.99 \sqrt{\frac{s_f - s_0}{s_f}} \right]. \qquad (4i)$$

In Eq. (4i), a factor of 0.99 is used instead of 0.97 originally adopted in Yuan et al. [16]. The former implies that the effective bond length is one at which 99% of the bond strength of an infinitely long bonded joint is achieved while the latter requires only 97%. The former is thus a more stringent definition and leads to effective bond lengths in closer agreement with those given by Chen and Teng's bond-strength model [7]. The effective bond length factor β_l in Eq. (4e) has been defined by Chen and Teng [7] to be

$$\beta_l = \sin\left(\frac{\pi L}{2 L_e} \right) \qquad \text{if } L \leq L_e. \qquad (4j)$$

The use of a sine function has its basis in the analytical solution [16]. The following alternative expression for β_l proposed by Neubauer et al. [29] provides similar predictions (Fig. 10):

$$\beta_l = \frac{L}{L_e}\left(2 - \frac{L}{L_e} \right) \qquad \text{if } L \leq L_e. \qquad (4k)$$

When compared with the present finite element results, Eq. (4k) is slightly more accurate (Fig. 10) but this small difference is insignificant and does mean that it provides more accurate predictions of test results. The use of either expression is thus satisfactory for design purposes, although Eq. (4k) was used with Eq. (4e) in the present study to obtain the results shown in Table 3.

Two of the three bond–slip models proposed in this study are compared with the four existing bond–slip models developed for normal-adhesive bonded joints in Fig. 4. It can be seen that Nakaba et al.'s model [12] and Savioa et al.'s model [36] are closer to the proposed models than the other two models. The maximum bond stress and the interfacial fracture energy of Nakaba et al.'s model and those of Savioa et al.'s model are however much larger than those of the proposed models.

8. Accuracy of the proposed models

8.1. Bond strength

In Fig. 11, the bond strengths predicted using the proposed bond–slip models are compared with the results

Fig. 12. Axial strains in FRP plate: test results versus predictions of proposed bond–slip models.

of the 253 pull tests listed in Table A.1. It can be found that the proposed bond–slip models give results in close agreement with the test results and perform better than existing bond–slip models. The results of the precise model and the simplified model are almost the same, with the precise model performing very slightly better. The ave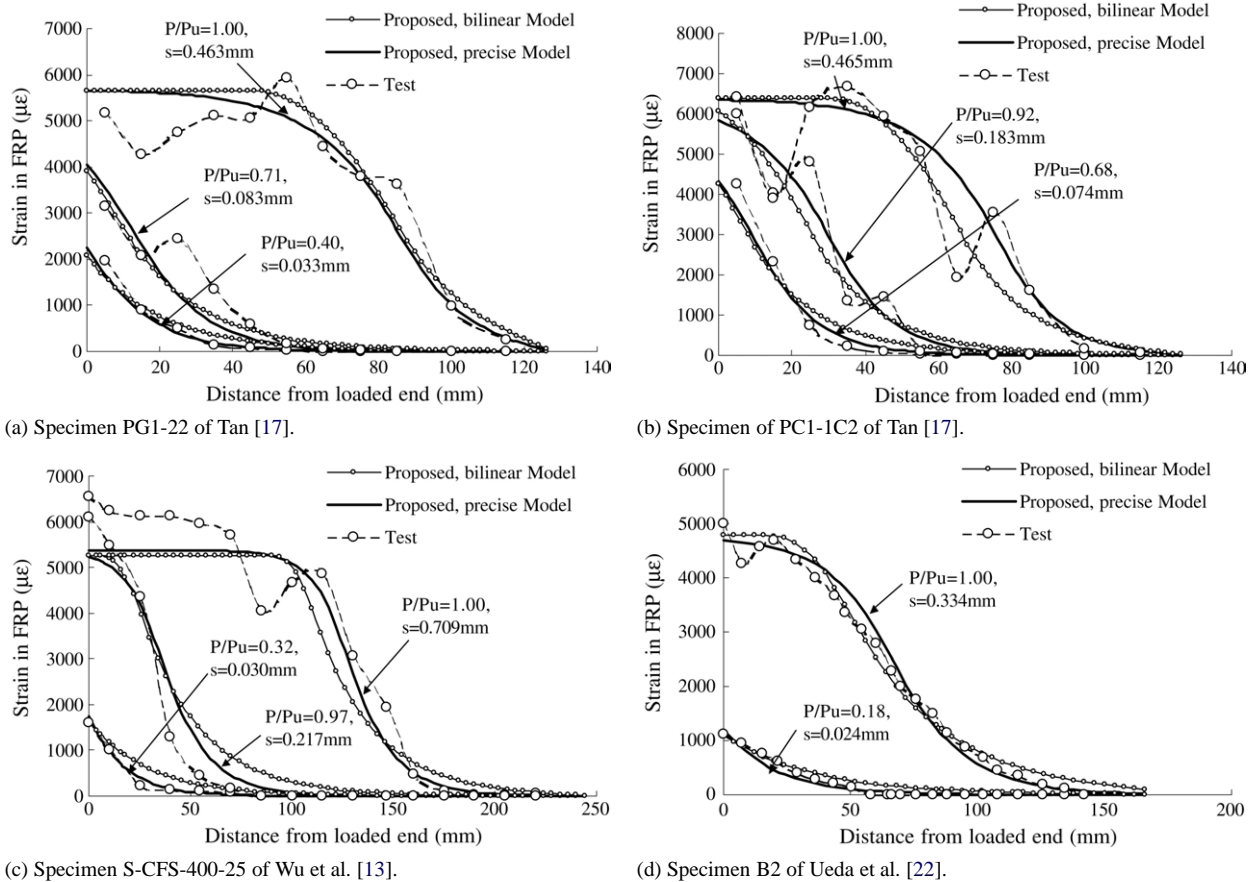rage value and coefficient of variation of the predicted-to-test bond strength ratios together with the correlation coefficient for the bond strength formula (Eq. (4e)) are given in Table 3. It can be seen that Eq. (4e) performs significantly better than all existing bond strength models except Chen and Teng's model [7]. The new bond strength model is only slightly better than Chen and Teng's model [7], so Chen and Teng's model [7] is still recommended for use in design due to its simple form.

8.2. Strain distributions in the FRP plate

The strain distributions in the FRP plate can be numerically calculated from the bond–slip models. The comparison of strain distributions between tests and predictions for specimens PG1-22 and PC1-1C2 tested by Tan [17], specimen S-CFS-400-25 tested by Wu et al. [13], and specimen B2, tested by Ueda et al. [22], are shown in Fig. 12(a)–(d). Comparisons are made for the same

applied load (except for insignificant differences as the test load levels are not identical to the load levels in the numerical analysis which was conducted by displacement control) before debonding and for the same effective stress transfer length in the stage of debonding propagation. The load levels and slip values indicated here are those from numerical analysis. It can be found that both the precise model and the bilinear model are in close agreement with the test results. The precise model does provide slightly more accurate predictions, which demonstrates that the curved shape of the precise model is closer to the real situation. Additional comparisons not reported here for a number of other specimens for which strain distributions are available also showed similar agreement.

Using specimen PG1-22 as an example, the strain distributions predicted with different bond–slip models are compared with the test results in Fig. 13. Comparisons are made for the same load of $P/P_u = 0.40$ (where P_u is the finite element ultimate load) before debonding occurs (Fig. 13(a)) and for the same effective stress transfer length of 125 mm in the stage of debonding propagation (Fig. 13(b)). It can be seen that at a low load in the pre-debonding stage, the strain distribution does not appear to be so sensitive to the bond–slip model. However, in the stage of debonding propagation, the differences between the models

(a) Before debonding stage.
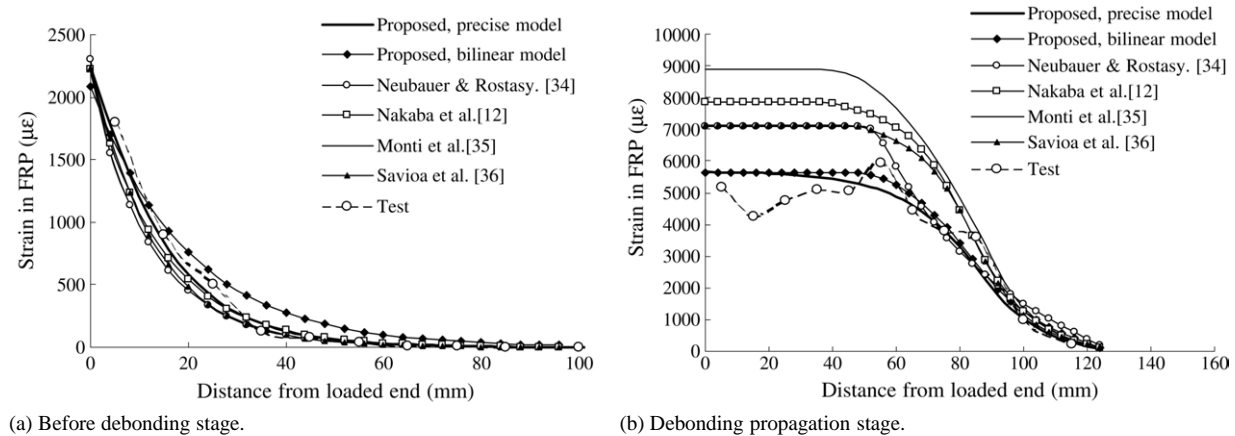
(b) Debonding propagation stage.

Fig. 13. Axial strains in FRP plate: test results versus predictions of all bond–slip models.

and between the model predictions and the test results are large. Fig. 13 shows that the existing models do not provide accurate predictions of test results.

9. Conclusions

This paper has provided a critical review and assessment of existing bond strength models and bond–slip models, and presented a set of three new bond–slip models. The assessment of theoretical models has been conducted using the test results of 253 pull specimens collected from the existing literature. The development of the new bond–slip models employed a new approach in which meso-scale finite element results with appropriate numerical smoothing are exploited together with test results. Based on the results and discussions presented in this paper, the following conclusions may be drawn.

1. Among the 12 existing bond strength models, the model proposed by Chen and Teng [7] is the most accurate. The bond strength model based on the proposed bilinear bond–slip model is as accurate as Chen and Teng's model [7] but is more complicated. Chen and Teng's model therefore remains the model of choice for use in design.
2. Typical bond–slip curves should consist of an ascending branch with continuous stiffness degradation to the maximum bond stress and a curved descending branch reaching a zero bond stress at a finite value of slip.
3. While a precise bond–slip model should consist of a curved ascending branch and a curved descending branch, other shapes such as a bilinear model can be used as a good approximation. An accurate bond–slip model should provide close predictions of both the shape and fracture energy (area under the bond–slip curve) of the bond–slip curve. None of the existing bond–slip models provides accurate predictions of both the shape and the interfacial fracture energy as found from tests.
4. The three new bond–slip models, based on a combination of finite element results and the test results predict both

the bond strength and strain distribution in the FRP plate accurately. These models are therefore recommended for future use in the numerical modelling of FRP-strengthened RC structures.

It should be noted that the scope of the present study has been limited to FRP-to-concrete bonded joints whose shear-deformed adhesive layer has a shear stiffness of no less than 2.5 GPa/mm. The studies by Dai and Ueda [14] and Ueda et al. [15] should be consulted for information on FRP-to-concrete bonded joints with a very soft adhesive layer. The present work nevertheless is believed to be applicable to at least all commercially available FRP systems for external bonding applications outside Japan.

Appendix A. Database of pull tests

See Table A.1.

Appendix B. Bond strength models

This appendix provides a summary of four bond strength models which are believed to be not widely accessible for the convenience of readers. Three of them are described in a recent JCI report [32] while the fourth one was developed in China. The following units are used: N for forces, MPa for stresses and elastic moduli, and mm for lengths.

Table A.1
Database of pull tests

Source	Specimen	FRP plate					Concrete prism[b]			Ultimate load P_u (kN)
		Thickness t_f (mm)	Width b_f (mm)	Bond length L (mm)	Elastic modulus E_f (GPa)	Tensile strength f_f (MPa)	Cube strength f_{cu} (MPa)	Tensile strength f_t (MPa)	Width b_c (mm)	
Tan [17]	PG1-11	0.169	50	130	97	2777	37.60	2.90	100	7.78[a]
	PG1-12	0.169	50	130	97	2777	37.60	2.90	100	9.19[a]
	PG1-1W1	0.169	75	130	97	2777	37.60	2.90	100	10.11[a]
	PG1-1W2	0.169	75	130	97	2777	37.60	2.90	100	13.95[a]
	PG1-1L11	0.169	50	100	97	2777	37.60	2.90	100	6.87[a]
	PG1-1L12	0.169	50	100	97	2777	37.60	2.90	100	9.20[a]
	PG1-1L21	0.169	50	70	97	2777	37.60	2.90	100	6.46[a]
	PG1-1L22	0.169	50	70	97	2777	37.60	2.90	100	6.66[a]
	PG1-21	0.338	50	130	97	2777	37.60	2.90	100	10.49[a]
	PG1-22	0.338	50	130	97	2777	37.60	2.90	100	11.43[a]
	PC1-1C1	0.111	50	130	235	3500	37.60	2.90	100	7.97[a]
	PC1-1C2	0.111	50	130	235	3500	37.60	2.90	100	9.19[a]
Zhao et al. [21]	NJ2	0.083	100	100	240	3550	20.50	2.08	150	11.00
	NJ3	0.083	100	150	240	3550	20.50	2.08	150	11.25
	NJ4	0.083	100	100	240	3550	36.70	2.87	150	12.50
	NJ5	0.083	100	150	240	3550	36.70	2.87	150	12.25
	NJ6	0.083	100	150	240	3550	36.70	2.87	150	12.75
Takeo et al. [20]	1-11	0.167	40	100	230	3481	36.56	2.86	100	8.75
	1-12	0.167	40	100	230	3481	33.75	2.74	100	8.85
	1-21	0.167	40	200	230	3481	36.56	2.86	100	9.30
	1-22	0.167	40	200	230	3481	33.75	2.74	100	8.50
	1-31	0.167	40	300	230	3481	36.56	2.86	100	9.30
	1-32	0.167	40	300	230	3481	33.75	2.74	100	8.30
	1-41	0.167	40	500	230	3481	36.56	2.86	100	8.05
	1-42	0.167	40	500	230	3481	36.56	2.86	100	8.05
	1-51	0.167	40	500	230	3481	33.50	2.73	100	8.45
	1-52	0.167	40	500	230	3481	33.50	2.73	100	7.30
	2-11	0.167	40	100	230	3481	31.63	2.64	100	8.75
	2-12	0.167	40	100	230	3481	31.63	2.64	100	8.85
	2-13	0.167	40	100	230	3481	33.13	2.71	100	7.75
	2-14	0.167	40	100	230	3481	33.13	2.71	100	7.65
	2-15	0.167	40	100	230	3481	30.88	2.61	100	9.00
	2-21	0.334	40	100	230	3481	31.63	2.64	100	12.00
	2-22	0.334	40	100	230	3481	31.63	2.64	100	10.80
	2-31	0.501	40	100	230	3481	31.63	2.64	100	12.65
	2-32	0.501	40	100	230	3481	31.63	2.64	100	14.35
	2-41	0.165	40	100	373	2942	30.88	2.61	100	11.55
	2-42	0.165	40	100	373	2942	30.88	2.61	100	11.00
	2-51	0.167	40	100	230	3481	33.13	2.71	100	9.85
	2-52	0.167	40	100	230	3481	33.13	2.71	100	9.50
	2-61	0.167	40	100	230	3481	33.13	2.71	100	8.80
	2-62	0.167	40	100	230	3481	33.13	2.71	100	9.25
	2-71	0.167	40	100	230	3481	33.13	2.71	100	7.65
	2-72	0.167	40	100	230	3481	33.13	2.71	100	6.80
	2-81	0.167	40	100	230	3481	63.25	3.87	100	7.75
	2-82	0.167	40	100	230	3481	63.25	3.87	100	8.05
	2-91	0.167	40	100	230	3481	30.88	2.61	100	6.75
	2-92	0.167	40	100	230	3481	30.88	2.61	100	6.80
	2-101	0.111	40	100	230	3481	31.63	2.64	100	7.70
	2-102	0.111	40	100	230	3481	33.13	2.71	100	6.95
Ren [23]	DLUT15-2G	0.507	20	150	83.03	3271	28.70	2.50	150	5.81
	DLUT15-5G	0.507	50	150	83.03	3271	28.70	2.50	150	10.60
	DLUT15-7G	0.507	80	150	83.03	3271	28.70	2.50	150	18.23
	DLUT30-1G	0.507	20	100	83.03	3271	45.30	3.22	150	4.63
	DLUT30-2G	0.507	20	150	83.03	3271	45.30	3.22	150	5.77
	DLUT30-3G	0.507	50	60	83.03	3271	45.30	3.22	150	9.42

Table A.1 (continued)

Source	Specimen	FRP plate					Concrete prism[b]			Ultimate load P_u (kN)
		Thickness t_f (mm)	Width b_f (mm)	Bond length L (mm)	Elastic modulus E_f (GPa)	Tensile strength f_f (MPa)	Cube strength f_{cu} (MPa)	Tensile strength f_t (MPa)	Width b_c (mm)	
	DLUT30-4G	0.507	50	100	83.03	3271	45.30	3.22	150	11.03
	DLUT30-6G	0.507	50	150	83.03	3271	45.30	3.22	150	11.80
	DLUT30-7G	0.507	80	100	83.03	3271	45.30	3.22	150	14.65
	DLUT30-8G	0.507	80	150	83.03	3271	45.30	3.22	150	16.44
	DLUT50-1G	0.507	20	100	83.03	3271	55.50	3.60	150	5.99
	DLUT50-2G	0.507	20	150	83.03	3271	55.50	3.60	150	5.90
	DLUT50-4G	0.507	50	100	83.03	3271	55.50	3.60	150	9.84
	DLUT50-5G	0.507	50	150	83.03	3271	55.50	3.60	150	12.28
	DLUT50-6G	0.507	80	100	83.03	3271	55.50	3.60	150	14.02
	DLUT50-7G	0.507	80	150	83.03	3271	55.50	3.60	150	16.71
	DLUT15-2C	0.33	20	150	207	3890	28.70	2.50	150	5.48
	DLUT15-5C	0.33	50	150	207	3890	28.70	2.50	150	10.02
	DLUT15-7C	0.33	80	150	207	3890	28.70	2.50	150	19.27
	DLUT30-1C	0.33	20	100	207	3890	45.30	3.22	150	5.54
	DLUT30-2C	0.33	20	150	207	3890	45.30	3.22	150	4.61
	DLUT30-4C	0.33	50	100	207	3890	45.30	3.22	150	11.08
	DLUT30-5C	0.33	50	100	207	3890	45.30	3.22	150	16.10
	DLUT30-6C	0.33	50	150	207	3890	45.30	3.22	150	21.71
	DLUT30-7C	0.33	80	100	207	3890	45.30	3.22	150	22.64
	DLUT50-1C	0.33	20	100	207	3890	55.50	3.60	150	5.78
	DLUT50-4C	0.33	50	100	207	3890	55.50	3.60	150	12.95
	DLUT50-5C	0.33	50	150	207	3890	55.50	3.60	150	16.72
	DLUT50-6C	0.33	80	100	207	3890	55.50	3.60	150	16.24
	DLUT50-7C	0.33	80	150	207	3890	55.50	3.60	150	22.80
Ueda et al. [22]	Ueda_A1	0.11	50	75	230	3479	29.74	2.55	100	6.25[a]
	Ueda_A2	0.11	50	150	230	3479	52.31	3.48	100	9.2[a]
	Ueda_A3	0.11	50	300	230	3479	52.31	3.48	100	11.95[a]
	Ueda_A4	0.22	50	75	230	3479	55.51	3.60	100	10.00[a]
	Ueda_A5	0.11	50	150	230	3479	54.36	3.56	100	7.30[a]
	Ueda_A6	0.165	50	65	372	2940	54.36	3.56	100	9.55[a]
	Ueda_A7	0.22	50	150	230	3479	54.75	3.57	100	16.25[a]
	Ueda_A8	0.11	50	700	230	3479	54.75	3.57	100	11.00[a]
	Ueda_A9	0.11	50	150	230	3479	51.03	3.43	100	10.00[a]
	Ueda_A10	0.11	10	150	230	3479	30.51	2.59	100	2.40[a]
	Ueda_A11	0.11	20	150	230	3479	30.51	2.59	100	5.35[a]
	Ueda_A12	0.33	20	150	230	3479	30.51	2.59	100	9.25[a]
	Ueda_A13	0.55	20	150	230	3479	31.67	2.64	100	11.75[a]
	Ueda_B1	0.11	100	200	230	3479	31.67	2.64	500	20.60
	Ueda_B2	0.33	100	200	230	3479	52.44	3.49	500	38.00
	Ueda_B3	0.33	100	200	230	3479	58.85	3.71	500	34.10
Wu et al. [13]	D-CFS-150-30a	0.083	100	300	230	4200	58.85	3.71	100	12.20[a]
	D-CFS-150-30b	0.083	100	300	230	4200	73.85	4.21	100	11.80[a]
	D-CFS-150-30c	0.083	100	300	230	4200	73.85	4.21	100	12.25[a]
	D-CFS-300-30a	0.167	100	300	230	4200	73.85	4.21	100	18.90[a]
	D-CFS-300-30b	0.167	100	300	230	4200	73.85	4.21	100	16.95[a]
	D-CFS-300-30c	0.167	100	300	230	4200	73.85	4.21	100	16.65[a]
	D-CFS-600-30a	0.333	100	300	230	4200	73.85	4.21	100	25.65[a]
	D-CFS-600-30b	0.333	100	300	230	4200	73.85	4.21	100	25.35[a]
	D-CFS-600-30c	0.333	100	300	230	4200	73.85	4.21	100	27.25[a]
	D-CFM-300-30a	0.167	100	300	390	4400	73.85	4.21	100	19.50[a]
	D-CFM-300-30b	0.167	100	300	390	4400	73.85	4.21	100	19.50[a]
	D-AR-280-30a	1	100	300	23.9	4400	73.85	4.21	100	12.75[a]
	D-AR-280-30b	1	100	300	23.9	4400	73.85	4.21	100	12.85[a]
	D-AR-280-30c	1	100	300	23.9	4400	73.85	4.21	100	11.90[a]
	S-CFS-400-25a	0.222	40	250	230	4200	73.85	4.21	100	15.40
	S-CFS-400-25b	0.222	40	250	230	4200	73.85	4.21	100	13.90
	S-CFS-400-25c	0.222	40	250	230	4200	73.85	4.21	100	13.00

Table A.1 (continued)

Source	Specimen	FRP plate					Concrete prism[b]			Ultimate load P_u (kN)
		Thickness t_f (mm)	Width b_f (mm)	Bond length L (mm)	Elastic modulus E_f (GPa)	Tensile strength f_f (MPa)	Cube strength f_{cu} (MPa)	Tensile strength f_t (MPa)	Width b_c (mm)	
	S-CFM-300-25a	0.167	40	250	390	4400	73.85	4.21	100	12.00
	S-CFM-300-25b	0.167	40	250	390	4400	73.85	4.21	100	11.90
	S-CFM-900-25a	0.5	40	250	390	4400	73.85	4.21	100	25.90
	S-CFM-900-25b	0.5	40	250	390	4400	73.85	4.21	100	23.40
	S-CFM-900-25c	0.5	40	250	390	4400	73.85	4.21	100	23.70

[a] Double-shear test; P_u is equal to half of the total applied load at failure.

[b] If the literature provides only the cylinder strength, then $f_{cu} = f_c'/0.78$. The tensile strength was found using $f_t = 0.395(f_{cu})^{0.55}$ according to the Chinese code [24]. The elastic modulus which is not listed in the table was found using $E_c = \frac{100\,000}{2.2+34.74/f_{cu}}$ according to the same code when needed.

B.1. Izumo's model

The bond strength model proposed by Izumo [32] is given by

$$P_u = (3.8 f_c'^{2/3} + 15.2) L E_f b_f t_f \times 10^{-3}$$

for carbon fibre sheets

and

$$P_u = (3.4 f_c'^{2/3} + 69) L E_f b_f t_f \times 10^{-3}$$

for aramid fibre sheets.

B.2. Sato's model

The bond strength model given by Sato [32] is described by the following equations:

$$\tau_u = 2.68 f_c'^{0.2} t_f E_f \times 10^{-5}$$
$$L_e = 1.89(E_f t_f)^{0.4}$$

if $L_e > L$, then $L_e = L$

$$P_u = (b_f + 2\Delta b) L_e \tau_u$$

$\Delta b = 3.7$ mm is the working width of concrete.

B.3. Iso's model

The bond strength model proposed by M. Iso [32] is given by

$$\tau_u = 0.93 f_c'^{0.44}$$
$$L_e = 0.125(E_f t_f)^{0.57}$$
$$P_u = \tau_u \times b_f \times L_e$$

where if $L_e = L$ if $L_e > L$.

B.4. Yang's model

The bond strength model proposed by Yang et al. [33] is

$$P_u = \left(0.5 + 0.08\sqrt{\frac{E_f t_f}{100 f_t}}\right) b_f L_e \tau_u$$

where

$$\tau_u = 0.5 f_t$$
$$L_e = 100 \text{ mm}.$$

References

[1] Teng JG, Chen JF, Simth ST, Lam L. FRP-strengthened RC structures. UK: John Wiley & Sons; 2002.

[2] Smith ST, Teng JG. FRP-strengthened RC structures-I: review of debonding strength models. Engineering Structures 2002;24(4): 385–95.

[3] Smith ST, Teng JG. FRP-strengthened RC structures-II: assessment of debonding strength models. Engineering Structures 2002;24(4): 397–417.

[4] Smith ST, Teng JG. Shear-bending interaction in debonding failures of FRP-plated RC beams. Advances in Structural Engineering 2003; 6(3):183–99.

[5] Teng JG, Smith ST, Yao J, Chen JF. Intermediate crack-induced debonding in RC beams and slabs. Construction and Building Materials 2003;17(6–7):447–62.

[6] Oehler DJ, Park SM, Mohamed Ali MS. A structural engineering approach to adhesive bonding longitudinal plates to RC beams and slabs. Composites: Part A 2003;34(12):887–97.

[7] Chen JF, Teng JG. Anchorage strength models for FRP and steel plates bonded to concrete. Journal of Structural Engineering, ASCE 2001; 127(7):784–91.

[8] Yao J, Teng JG, Chen JF. Experimental study on FRP-to-concrete bonded joints. Composites-Part B: Engineering 2005;36(2):99–113.

[9] Maeda T, Asano Y, Sato Y, Ueda T, Kakuta Y. A study on bond mechanism of carbon fiber sheet. In: Proc. of 3rd international symposium on non-metallic (FRP) reinforcement for concrete structures, vol. 1. Sapporo: Japan Concrete Institute; 1997. p. 279–85.

[10] Brosens K, van Gemert D. Anchoring stresses between concrete and carbon fiber reinforced laminates. In: Proc. of 3rd international symposium on non-metallic (FRP) reinforcement for concrete structures, vol. 1. Sapporo: Japan Concrete Institute; 1997. p. 271–8.

[11] De Lorezis L, Miller B, Nanni A. Bond of fiber-reinforced polymer laminates to concrete. ACI Material Journal 2001;98(3):256–64.

[12] Nakaba K, Toshiyuki K, Tomoki F, Hiroyuki Y. Bond behavior between fiber-reinforced polymer laminates and concrete. ACI Structural Journal 2001;98(3):359–67.

[13] Wu ZS, Yuan H, Hiroyuki Y, Toshiyuki K. Experimental/analytical study on interfacial fracture energy and fracture propagation along FRP-concrete interface. In: ACI International SP-201-8. 2001. p. 133–52.

[14] Dai JG, Ueda T. Local bond stress slip relations for FRP sheets-concrete interfaces. In: Proc. of 6th international symposium on FRP reinforcement for concrete structures. Singapore: World Scientific Publications; 2003. p. 143–52.

[15] Ueda T, Dai JG, Sato Y. A nonlinear bond stress–slip relationship for FRP sheet–concrete interface. In: Proc. of international symposium on latest achievement of technology and research on retrofitting concrete structures. 2003. p. 113–20.

[16] Yuan H, Teng JG, Seracino R, Wu ZS, Yao J. Full-range behavior of FRP-to-concrete bonded joints. Engineering Structures 2004;26(5):553–64.

[17] Tan Z. Experimental research for RC beam strengthened with GFRP. Master thesis, China: Tsinghua University; 2002 [in Chinese].

[18] Chajes MJ, Finch WWJ, Januszka TF, Thonson TAJ. Bond and force transfer of composite material plates bonded to concrete. ACI Structural Journal 1996;93(2):295–303.

[19] Taljsten B. Defining anchor lengths of steel and CFRP plates bonded to concrete. International Journal of Adhesion and Adhesives 1997; 17(4):319–27.

[20] Takeo K, Matsushita H, Makizumi T, Nagashima G. Bond characteristics of CFRP sheets in the CFRP bonding technique. In: Proc. of Japan concrete institute, vol. 19, no. 2. June, 1997. p. 1599–604.

[21] Zhao HD, Zhang Y, Zhao M. Research on the bond performance between CFRP plate and concrete. In: Proc. of 1st conference on FRP-concrete structures of China. 2000. p. 247–53.

[22] Ueda T, Sato Y, Asano Y. Experimental study on bond strength of continuous carbon fiber sheet. In: Proc. of 4th international symposium on fiber reinforced polymer reinforcement for reinforced concrete structures, SP-188. Farmington Hills (MI): ACI; 1999. p. 407–16.

[23] Ren HT. Study on basic theories and long time behavior of concrete structures strengthened by fiber reinforced polymers. Ph.D. thesis. China: Dalian University of Technology; 2003 [in Chinese].

[24] GB 50010. Code for design of concrete structures. Beijing: China Building Industry Press; 2002 [in Chinese].

[25] Tanaka T. Shear resisting mechanism of reinforced concrete beams with CFS as shear reinforcement. Graduation thesis. Japan: Hokkaido University; 1996.

[26] Hiroyuki Y, Wu Z. Analysis of debonding fracture properties of CFS strengthened member subject to tension. In: Proc. of 3rd international symposium on non-metallic (FRP) reinforcement for concrete structures, vol. 1. 1997. p. 284–94.

[27] van Gemert D. Force transfer in epoxy-bonded steel–concrete joints. International Journal of Adhesion and Adhesives 1980;1:67–72.

[28] Brosens K, van Gemert D. Anchorage design for externally bonded carbon fiber reinforced polymer laminates. In: Proc. of 4th international symposium on fiber reinforced polymer reinforcement for reinforced concrete structures, SP-188. Farmington Hills (MI): ACI; 1999. p. 635–45.

[29] Neubauer U, Rostasy FS. Design aspects of concrete structures strengthened with externally bonded CFRP plates. In: Proc. of 7th international conference on structural faults and repair, vol. 2. Edinburgh (Scotland): ECS Publications; 1997. p. 109–18.

[30] Khalifa A, Gold WJ, Nanni A, Aziz A. Contribution of externally bonded FRP to shear capacity of RC flexural members. Journal of Composites for Construction, ASCE 1998;2(4):195–203.

[31] Chaallal O, Nollet MJ, Perraton D. Strengthening of reinforced concrete beams with externally bonded fiber-reinforced-plastic plates: design guidelines for shear and flexure. Canadian Journal of Civil Engineering 1998;25(4):692–704.

[32] JCI. Technical report of technical committee on retrofit technology. In: Proc., international symposium on latest achievement of technology and research on retrofitting concrete structures. 2003.

[33] Yang YX, Yue QR, Hu YC. Experimental study on bond performance between carbon fiber sheets and concrete. Journal of Building Structures 2001;22(3):36–42 [in Chinese].

[34] Neubauer U, Rostasy FS. Bond failure of concrete fiber reinforced polymer plates at inclined cracks-experiments and fracture mechanics model. In: Proc. of 4th international symposium on fiber reinforced polymer reinforcement for reinforced concrete structures, SP-188. Farmington Hills (MI): ACI; 1999. p. 369–82.

[35] Monti M, Renzelli M, Luciani P. FRP adhesion in uncracked and cracked concrete zones. In: Proc. of 6th international symposium on FRP reinforcement for concrete structures. Singapore: World Scientific Publications; 2003. p. 183–92.

[36] Savioa M, Farracuti B, Mazzotti D. Non-linear bond–slip law for FRP-concrete interface. In: Proc. of 6th international symposium on FRP reinforcement for concrete structures. Singapore: World Scientific Publications; 2003. p. 163–72.

[37] Taljsten B. Plate bonding: strengthening of existing concrete structures with epoxy bonded plates of steel or fiber reinforced plastics. Ph.D. thesis. Sweden: Lulea University of Technology; 1994.

[38] Wu ZS, Yuan H, Niu HD. Stress transfer and fracture propagation in different kinds of adhesive joints. Journal of Engineering Mechanics, ASCE 2002;128(5):562–73.

[39] MSC.Marc. User's manual. MSC Software Corporation; 2003.

[40] Lu XZ, Ye LP, Teng JG, Jiang JJ. Meso-scale finite element model for FRP plates/sheets bonded to concrete. Engineering Structures 2005; 27(4):564–75.

[41] Rots JG, Blaauwendraad J. Crack models for concrete: discrete or smeared? fixed, multi-directional or rotating? Heron 1989;34(1).